ELSEVIER

The frictional sliding response of elasto-plastic materials in contact with a conical indenter

S. Bellemare, M. Dao, S. Suresh *

*Department of Materials Science and Engineering, Massachusetts Institute of Technology, 77 Massachusetts Avenue,
Rm 4-140, Cambridge MA 02139, United States*

Abstract

Over the past decade, many computational studies have explored the mechanics of normal indentation. Quantitative relationships have been well established between the load–displacement hysteresis response and material properties. By contrast, very few studies have investigated broad quantitative aspects of the effects of material properties, especially plastic deformation characteristics, on the frictional sliding response of metals and alloys. The response to instrumented, depth-sensing frictional sliding, hereafter referred to as a scratch test, could potentially be used for material characterization. In addition, it could reproduce a basic tribological event, such as asperity contact and deformation, at different length scales for the multi-scale modeling of wear processes. For these reasons, a comprehensive study was undertaken to investigate the effect of elasto-plastic properties, such as flow strength and strain hardening, on the response to steady-state frictional sliding. Dimensional analysis was used to define scaling variables and universal functions. The dependence of these functions on material properties was assessed through a detailed parametric study using the finite element method. The strain hardening exponent was found to have a greater influence on the scratch hardness and the pile-up height during frictional sliding than observed in frictionless normal indentation. When normalized by the penetration depth, the pile-up height can be up to three times larger in frictional sliding than in normal indentation. Furthermore, in contrast to normal indentation, sink-in is not observed during frictional sliding over the wide range of material properties examined. Finally, friction between indenter and indented material was introduced in the finite element model, and quantitative relationships were also established for the limited effects of plastic strain hardening and yield strength on the overall friction coefficient. Aspects of the predictions of computational simulations were compared with experiments on carefully selected metallic systems in which the plastic properties were systematically controlled. The level of accuracy of the predicted frictional response is also assessed by recourse to the finite element method and by comparison with experiment.
© 2006 Elsevier Ltd. All rights reserved.

Keywords: Scratch test; Indentation; Elasto-plastic properties; Dimensional analysis; Finite element method; Scratch hardness; Pile-up height

* Corresponding author. Tel./fax: +1 617 253 3320.
  E-mail address: ssuresh@mit.edu (S. Suresh).

1. Introduction

The single asperity contact of a hard indenter on a softer material can generate a permanent impression. The dependence of geometry and material properties, on the size and morphology of this impression and on the extent of deformation surrounding it, has been the subject of technological and scientific interest over the past century. Although mechanics of deformation and material penetration and/or loss in a variety of localized contact conditions (Johnson, 1985) including frictional sliding or scratching (Williams, 1996) have been topics of scientific studies for many decades, normal indentation is by far the most commonly used technique to characterize the hardness of materials (Tabor, 1951; Fischer-Cripps, 2000). The different scales for hardness are all estimates for the average pressure of contact, but the reference contact area used to normalize the normal force varies significantly depending on the experimental methods employed and the details of the analysis. Although the hardness value depends on the definition of contact area and indenter geometry, conventional hardness test procedures are cost-effective and easy to implement. Consequently, indentation hardness measurements have been used very extensively not only for quality control (Revankar, 1990), but also as prime predictors of tribological resistance (Hutchings, 1992).

Over the past two decades, the development and commercialization of depth-sensing indentation instruments has facilitated the simultaneous measurement of the applied force and the induced displacement, providing for each test a force versus displacement hysteresis curve from loading and unloading. Significant theoretical and computational research have also been devoted to the establishment of relationships between the quantitative details of these force–displacement curves and the underlying elastic and plastic properties of the material being indented. For instance, the initial part of the unloading slope provides a measure of the elastic compliance that can be used to estimate the elastic modulus of indented materials (Oliver and Pharr, 1992). Other parameters such as the curvature of the loading curve and the residual depth upon complete unloading can be used to estimate the hardness and the yield strength without measuring the contact area (Giannakopoulos and Suresh, 1999; Dao et al., 2001).

For instrumented sharp indentation, finite element simulations and dimensional analyses have been used in several studies to establish relationships between the hysteresis curves and the elasto-plastic properties of materials (Cheng and Cheng, 1998a,b; Dao et al., 2001; Cheng et al., 2002; Ogasawara et al., 2005; Wang et al., 2005; Wang and Rokhlin, 2005). To determine with a reasonable precision the initial yield strength and the strain hardening exponent, recent studies have examined the potential advantage of using two different indenter geometries to characterize the plastic properties (Bucaille et al., 2003; Chollacoop et al., 2003; Cao and Lu, 2004a,b). Changing the tip angle changes the magnitude of the average plastic strain, therefore providing more information about the evolution of the flow stress with the plastic strain (Atkins and Tabor, 1965; Milman et al., 1993). As an alternative technique to determine the plastic flow properties accurately, one can use a single indenter and measure directly characteristic parameters of the residual indent profile (Tunvisut et al., 2001; Matsuda, 2002; Tunvisut et al., 2002; Sakai et al., 2003). After the experiment such a technique requires to determine the surface profile, but it could also exploit the known effects of strain hardening exponent on pile-up morphology (Marx and Balke, 1997; Cheng and Cheng, 1998a,b; Alcala et al., 2000; Mata and Alcala, 2003). How pile-up and hardness each quantitatively dependent on individual elasto-plastic properties is now fairly well established for homogeneous materials subjected to sharp normal indentation.

As compared to normal indentation where the stress field is axisymmetric (for a spherical or a conical indenter), it requires more computational resources to study frictional sliding using finite element methods. The scratch loading mode was used for the establishment of the first hardness scale in the pioneering work of Mohs (1824), but the technique is mostly being used nowadays in specialized areas including the visual damage and wear of polymers (Briscoe et al., 1993; Dasari et al., 2004; Misra et al., 2004; Maeda et al., 2005; Mohamed Sani et al., 2005) and the tribological resistance of metallic-base composites (Zhang et al., 1994, 1995; Liang et al., 1995; Deuis et al., 1996; Wilson et al., 2000; Bolduc et al., 2003). The limited usage to characterize the plastic flow behavior is mostly due to the lack of an appropriate analytical framework to interpret frictional sliding experiments. During a frictional sliding test carried out under appropriate plasticity conditions and under a constant normal force, steady-state conditions are obtained for the penetration depth, the friction force and the pile-up after an initial transient regime. For this steady-state contact problem, analytical models have been developed based on the upper bound theorem, but the solution scheme requires

specification of the material flow velocity field (Williams, 1996). Using the finite element method, a number of recent studies have examined the effect of flow stress and tip geometry on the scratch response (Bucaille et al., 2001; Bucaille and Felder, 2002; Subhash and Zhang, 2002; Youn and Kang, 2004, 2005). However, we found only one study for which plastic strain hardening was included (Fang et al., 2005). In all cases, the number of material property sets studied was too limited to gain a broad fundamental understanding.

In this paper, we report results from a comprehensive computational study of frictional sliding in elasto-plastic materials. Similarly to the previous research summarized above, this study is based on continuum mechanics, homogeneous properties and size-scale independence. With no quantitative information available in the literature for the effects of plastic strain hardening and yield strength in steady-state frictional sliding conditions, this continuum-based approach was chosen to ascertain the usefulness of the information that can be obtained from frictional sliding and to compare it with normal indentation. Following an approach similar to that used in finite element studies of instrumented indentation, dimensional functions are derived for the steady-state regime of frictional sliding and the predictions are compared with experimental results in a model material system. The concept of a scratch hardness, extracted from instrumented frictional sliding experiments, is developed, and its relationship to indentation hardness is explored both experimentally and computationally.

2. Framework for the analysis

2.1. Problem formulation

The continuum-mechanics-based analysis focuses on the response of elasto-plastic materials in frictional sliding contact with a hard conical tip. It is possible in frictional sliding to reach a condition of constant penetration depth, normal force and tangential force. Both computationally and experimentally, this steady-state regime can be obtained through different paths including constant imposed normal force or constant imposed normal displacement. At least theoretically, the response in steady state should be path independent. In practice, steady state can be obtained in constant load-controlled conditions with fewer calibrations and calculations because there is no need to specify the tip trajectory based on surface position and machine/specimen compliance.

Throughout the simulation or experiment, it is possible to continuously monitor the normal contact force P, the normal indenter displacement h and the tangential or friction force F_t. As schematically shown in Fig. 1, a typical experiment involves indentation followed by a transient regime and a steady regime of frictional sliding. In the transient regime, the depth stabilizes to a constant value when a constant load is prescribed; whereas, the pile-up geometry and forces stabilizes to constant values when a constant penetration depth is imposed. Fig. 1 also illustrates the definition of the apex angle θ, the residual depth h_r and the residual pile-up height h_p. Under steady-state conditions, these parameters and the geometry of the pile-up become fixed. In addition to the known external variables, the friction coefficient μ_a between the indenter and the indented material and the elastic properties of the tip can also influence the steady-state geometry.

Knowing P, h_r, θ, F_t and the material properties for the indenter and the surface can fully specify this frictional sliding process. However, as for the indentation response, the normalized pile-up height h_p/h_r can vary significantly with material properties. The analysis here will specifically quantify this dependence for materials where the elastic and plastic response can be approximated, respectively, by Hooke's law and the von Mises yield criterion with isotropic power law hardening. Under those general conditions, the dependence of the true stress σ on the true strain ε is commonly expressed as (e.g., (Dao et al., 2001))

$$\sigma = \begin{cases} E\varepsilon & \text{for } \sigma \leqslant \sigma_y, \\ R\varepsilon^n & \text{for } \sigma > \sigma_y, \end{cases} \tag{1}$$

where E is the Young's modulus, R a strength coefficient, n the strain hardening exponent and σ_y the initial yield stress at zero offset strain. In this representation, the true strain ε is a uniaxial strain. The multiaxial stress state for frictional sliding will be introduced after a rearrangement of Eq. (1). The total true strain ε can be decomposed in elastic and plastic components to obtain

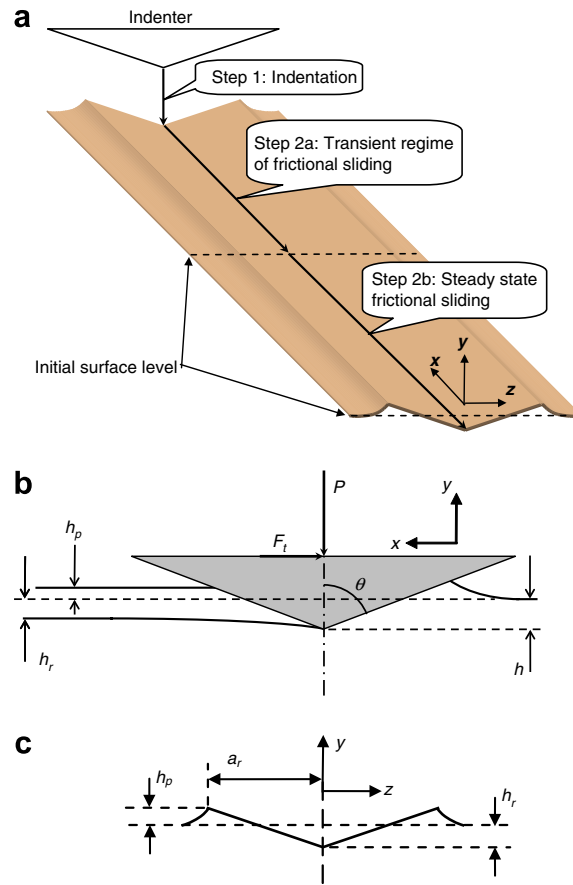$$\varepsilon = \varepsilon_y + \varepsilon_p. \tag{2}$$

Fig. 1. Problem definition and nomenclature: (a) A schematic of the frictional sliding process, (b) a cross-sectional of the symmetry plane in the steady-state regime, and (c) a cross-sectional view of the residual scratch profile. All solid lines represent the top free surface of the material being plastically deformed.

For continuity when $\sigma = \sigma_y$, Eq. (1) requires that

$$\sigma_y = E\varepsilon_y = R\varepsilon_y^n, \tag{3}$$

when $\sigma > \sigma_y$, the substitution of Eqs. (2) and (3) in (1) leads to the replacement of the coefficient R by elastic properties and to express the flow stress constitutive relation as

$$\sigma = \sigma_y \left(1 + \frac{E}{\sigma_y} \varepsilon_p \right)^n. \tag{4}$$

The implementation of this relationship for the multiaxial stress state followed the concept of equivalent plastic strain and the incremental theory of plasticity. With a constitutive model at hand, the subsequent step consists in defining the physical quantities to describe the frictional sliding response. In contrast with normal indentation, the steady-state nature of the frictional sliding process does not allow us to probe the elastic recovery of the material using the normal force–normal displacement (P–h) hysteresis curve. Without knowledge of the unloading compliance in this elastic recovery in frictional sliding, the Young's modulus cannot be estimated through techniques such as those originally proposed for normal indentation (Oliver and Pharr, 1992, 2004; Pharr et al., 1992). A second and related limitation for frictional sliding involves the calculation of actual area of contact that is also typically obtained through an analysis of the (P–h) hysteresis curve. Alternative ways to estimate the actual area of contact include in situ imaging, but this solution would require advanced instrumentation, especially at low loads and is not always feasible under all test conditions.

The solution proposed here for measuring the contact area consists of probing directly the residual scratch width $2a_r$ through surface imaging or profilometry. Using profilometry, additional parameters such as h_p and h_r can be readily quantified and used in the analysis. Practical aspects associated with the measurement of these quantities are discussed in Section 3.3. Using this residual profile approach, the scratch hardness of the material can be directly calculated using the traditional definition of hardness (Tabor, 1951; Johnson, 1985; Williams, 1996; Fischer-Cripps, 2000)

$$H_s = \frac{P}{A_r}, \tag{5}$$

where A_r is an estimate of the residual projected area of contact. Following the same definition as in previous models for frictional sliding contact with hard indenters (Williams, 1996), A_r is defined as half the area of a circle of radius a_r,

$$A_r = (\pi/2)a_r^2. \tag{6}$$

2.2. Dimensional analysis

Dimensional analysis has proven to be useful to the study of the contact mechanics for instrumented normal indentation (Cheng and Cheng, 2004). Using a similar approach for the steady-state frictional sliding process allows us to present the results in a general form and to clearly state the dependence of each physical quantity on the material and geometrical parameters. Our independent physical quantities can be expressed as

$$P = P(a_r, E, v, \sigma_y, n, E_i, v_i, \theta, \mu_a), \tag{7}$$
$$h_p = h_p(h_r, E, v, \sigma_y, n, E_i, v_i, \theta, \mu_a), \tag{8}$$

and

$$F_t = F_t(P, E, v, \sigma_y, n, E_i, v_i, \theta, \mu_a), \tag{9}$$

where E_i and v_i are the Young's modulus and the Poisson's ratio, respectively, of the indenter. For the functional of the force P, the use of a_r instead of h_r was found to be more appropriate because experimental determination of h_r requires estimation of the position of original surface through an interpolation procedure which decreases the level of accuracy. Accuracy on a_r or h_r is important as the error is doubled in calculating the contact area.

The above functional relationships are often simplified (Johnson, 1985) by introducing the reduced Young's modulus for the combined indenter–substrate system as

$$E^* = \left[\frac{(1 - v^2)}{E} + \frac{(1 - v_i^2)}{E_i} \right]^{-1}. \tag{10}$$

Using this reduced modulus and applying the Π theorem of dimensional analysis, expressions (7)–(9), respectively, become

$$\frac{P}{\sigma_y a_r^2 (\pi/2)} = \Pi_\alpha \left(\frac{\sigma_y}{E^*}, n, \theta, \mu_a \right) = \frac{H_s}{\sigma_y}, \tag{11}$$
$$\frac{h_p}{h_r} = \Pi_\beta \left(\frac{\sigma_y}{E^*}, n, \theta, \mu_a \right), \tag{12}$$

and

$$\frac{F_t}{P} = \mu_{tot} = \Pi_\gamma \left(\frac{\sigma_y}{E^*}, n, \theta, \mu_a \right), \tag{13}$$

where Π_α, Π_β and Π_γ are general dimensionless functions. Several alternative expressions could be proposed but the one presented here allows for the dimensionless functions to directly correspond to simple and important ratios of measurable quantities, namely the normalized scratch hardness H_s/σ_y, the ratio of pile-up heights h_p/h_r and the overall friction coefficient μ_{tot}.

2.3. Computational models

For the analysis presented here, the material Poisson's ratio v was maintained at 0.3 while all the other material parameters were varied over a wide range (see Section 3.2). For the conical indenter, the model assumed elastic rigidity, and the apex angle θ was fixed at 70.3°. The contact of this indenter with the surface was assumed to follow Amonton's law of friction,

$$q = \mu_a p, \tag{14}$$

where q is the tangential traction and p is the local pressure or the normal traction. As in previous contact mechanics studies that included friction (Mesarovic and Fleck, 1999; Bucaille et al., 2003; Ogasawara et al., 2005) and based on experimental results reported elsewhere (Bowden and Tabor, 1950; Hanlon et al., 2005a,b), a value of 0.15 was used for μ_a. This value is believed to represent a typical contact condition between a diamond tip and the polished surface of a metal covered with a thin layer of natural oxides.

Full three-dimensional models were constructed because the stress and strain fields generated by frictional sliding cannot be approximated using two-dimensional or axisymmetric mesh domains. However, the plane defined by the normal to the surface and the sliding direction is a symmetry plane, which allows for solving only half of the full space. To further minimize the size of the problem, the meshing procedure involved the radial propagation of the seeds from the region of refined mesh. Fig. 2 presents the indenter, the mesh and the overall simulation domain. The domain consists in two main parts: a spherical section for the mesh located upstream with respect to the indenter position and a conical section for the material located downstream. The upstream configuration is significantly more efficient, but the meshing downstream needed to remain fully refined to capture with accuracy an unloaded profile. For more efficient convergence toward a steady-state solution, the initial stress-free mesh was generated with a preexisting scar, where the front end of the scar (half-cone shaped) is in conformal contact with the conical indenter at the beginning of the simulation. The complete mesh domain contains 170,000 reduced integration eight-noded elements.

The finite element computations were performed using the general purpose software package ABAQUS (ABAQUS Theory Manual Version 6.5, Hibbitt, Karlsson and Sorensen Inc, Pawtucket, 2005). Three
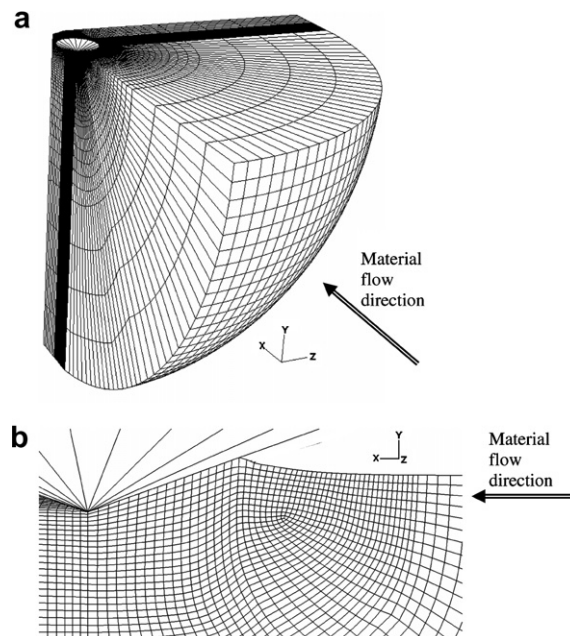

Fig. 2. (a) Overview of mesh and the complete simulation domain with the fixed conical indenter in the top left, the material flow direction along positive X direction and the symmetry plane at $Z = 0$. (b) Detailed view on the symmetry plane $Z = 0$ of the region near the indenter with the upstream direction to the right.

different solution schemes were used and compared for their time efficiency and accuracy. An explicit formulation with Eulerian boundary conditions was found to provide the most consistent results and enabled use of the smallest simulation domain. In this formulation, the material enters at a constant velocity through the upstream spherical surface, flows through the stationary mesh and exits downstream. The mesh adapts to geometrical changes induced by the frictional contact of the fixed indenter tip with the free surface.

The results from this explicit formulation were compared with elastic solutions and well tested for convergence. For an elastic frictional contact, the contact pressure distribution and the Von Mises stress distribution agreed within 5% error with known analytical and numerical solutions from previous studies (Truman et al., 1995; Fischer-Cripps, 2000; Storakers and Elaguine, 2005). With plasticity, the solution was determined to be independent of the far-field boundary conditions and insensitive to mesh size. In the range where 13–20 elements were within the contact radius created by the indenter, the main advantage of the finer mesh was for the determination of the pile-up height and the area of contact from the coordinates of the surface nodes. For all the simulation results presented here, 13 elements were in contact with the indenter in the initial non-deformed configuration. During the simulation, the number of elements increased further as the pile-up formed. In fact, the mesh was optimized with a greater refinement near the pile-up region than near the center of contact.

To further verify both the trends and the absolute value of the predictions from the explicit/Eulerian formulation, two additional sets of finite element models were constructed and simulation results were obtained to cover a wide range of material properties. The hardness and pile-up results matched within 2% error with those obtained using an explicit scheme with Lagrangian boundary conditions. Such a good correspondence provided conclusive evidence that using Eulerian boundaries allows for a reduction in the domain size without affecting the results obtained using explicit dynamic formulation. The second set of comparative results was based on a standard implicit solution scheme with Lagrangian boundary conditions. To limit the increase in the computational time associated with the use of an implicit algorithm and with the increased domain size, only 50,000 elements were used for these simulations. As reported in Table 1, the results show slightly greater differences with a maximum error of 10% for the normalized hardness. To minimize the time steps required to reach a steady-state regime, a small linear decrease in penetration depth was introduced for the first third of the scratching distance. For the remaining of the scratching distance, the depth was maintained constant and the steady state over a distance sufficient enough to extract an accurate residual profile. Without an initial regime with a decreasing depth, an apparent steady-state response was also reached but the residual pile-up height was found to be significantly lower as shown for two cases in Table 1. Part of this dependence on the trajectory could originate from the level of mesh refinement. However, even with the coarsest mesh cases, none of the explicit formulations exhibited a significant dependence on the initial scratching regime.

2.4. Experimental comparison

Frictional sliding experiments were carried out on three specimens of pure nickel with different grain sizes. These nickel specimens were already well characterized for grain size distribution and tensile properties in

Table 1
Comparison between the simulation results obtained using standard implicit and explicit schemes

σ_y/E	n	H_s/σ_y			h_p/h_r			μ_{tot}		
		Implicit	Explicit	Diff. (%)	Implicit	Explicit	Diff. (%)	Implicit	Explicit	Diff. (%)
0.001	0.1	4.6	4.3	7	0.70	0.75	−7	0.394	0.399	−1
0.001	0.2	8.3	7.8	6	0.56	0.60	−7	0.392	0.396	−1
0.001[a]	0.2	8.5	7.8	9	0.52	0.60	−13	0.392	0.396	−1
0.001	0.35	18.4	19.3	−5	0.39	0.38	3	0.400	0.385	4
0.001	0.5	40.8	41.2	−1	0.21	0.18	17	0.382	0.361	6
0.001[a]	0.5	41.1	41.2	0	0.17	0.18	−6	0.375	0.361	4
0.02	0.02	2.8	2.7	4	0.72	0.69	4	0.354	0.366	−3
0.02	0.1	3.6	3.4	6	0.54	0.49	10	0.351	0.361	−3
0.02	0.2	4.5	5.0	−10	0.43	0.39	10	0.343	0.348	−1

[a] Constant depth for the implicit scheme.

previous studies where, based on recent classification for grain size regimes (Kumar et al., 2003), they were appropriately labeled as microcrystalline (mc), ultra-fine crystalline (ufc) and nanocrystalline (nc) metals. All three specimens were mechanically polished down to a surface roughness of less than ±5 nm and tested on a commercial nanoindentation test system (Nanotest™, Micro Materials Ltd., Wrexham, United Kingdom). The scratch experiments were carried out under constant normal load. This load was applied through the interaction of a permanent magnet with the solenoid coil attached to the upper end of the pendulum. This pendulum is held in the center through a frictionless pivot and it holds the tip at the opposite end. Therefore, the force is applied in the upper part and transferred to the tip through the frictionless pivot. On the other hand, the tangential displacement sample was imposed by a stage micro-motor, and the tangential force was calculated from the strain in the elastic cantilever beam holding the tip. The conical diamond probe had an apex angle of 70.3° and a tip radius of 2 µm. For the purpose of the experimental comparison, the scale of experimentation is sufficiently large to consider the tip as perfectly conical. After the experiment, a series of at least 30 cross-sectional profiles of the residual steady-state scratch were obtained using a Tencor P10 pro-filometer (KLA-Tencor, San Jose, California) equipped with a conical diamond probe which had an apex angle of 45° and a tip radius of 2 µm.

3. Computational results

With the fine mesh and the explicit/Eulerian solution scheme, a comprehensive parametric study was conducted to quantify the effect of material properties on the frictional sliding response in steady state. The penetration depth of the indenter was kept constant during these simulations.

3.1. Forces and residual profiles

For a given set of material properties, Fig. 3 shows the force evolution and the total internal energy as a function of the magnitude of relative displacement between the indenter and the meshed domain of the substrate. The force results obtained from using an implicit scheme simulation are also included for comparison. In all cases, the normal and frictional forces are both normalized by the A_r obtained using the steady-state residual profile and Eq. (6). Hence, the final magnitude of the non-dimensional (normalized) normal force corresponds to the scratch hardness H_s. The relative displacement must exceed five times the radius of contact a_r before reaching steady-state conditions. With the Eulerian scheme, it takes a longer frictional traveling distance to reach steady state, but this increase is not at the expense of an increase in the size of the simulation domain. Once steady-state conditions are reached at the position of contact between the indenter and surface,
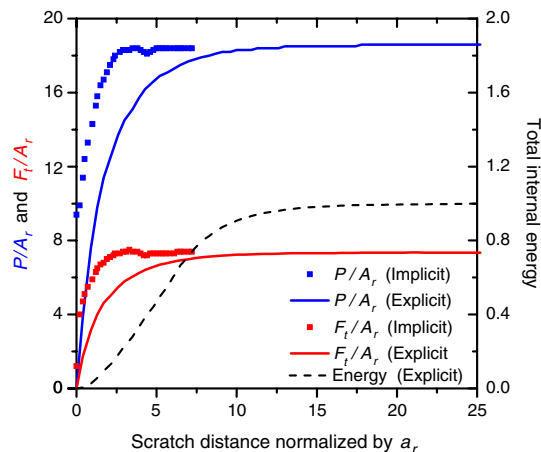

Fig. 3. Evolution of total normal and tangential interaction forces between the indenter and the surface for material parameters $\sigma_y/E^* = 0.001$ and $n = 0.35$. The lines are for the explicit/Eulerian solution scheme whereas the symbols are for independent calculations using the implicit scheme (included for comparison).

the simulation needs to be pursued further over at least three times the radius of contact in order to obtain an accurate steady-state surface profile after elastic recovery of the free surface. For the results obtained using the Eulerian scheme, the condition of steady state are fully satisfied throughout the domain when the total internal energy becomes constant. Stabilization of the total internal energy was used as a criterion to terminate the simulation.

A series of residual scratch profiles is shown in Fig. 4 to illustrate the strong influence of the strain hardening exponent n. The effect of the solution scheme is also shown in Fig. 4. The sliding direction is normal to this plot and the vertical axis corresponds to the symmetry plane. For a fixed ratio of $\sigma_y/E^* = 0.001$, the normalized pile-up height h_p/h_r increases gradually from approximately 0.20 to 0.75 as n decreases from 0.5 to 0.1. The height is approximately the same for the explicit and the implicit solutions, with differences that could be accounted for by mesh size. Also shown in Fig. 4 is a profile for an initial yield strength σ_y yield strength that is 20 times as large. Although both σ_y/E^* and n can influence h_p/h_r, the contribution from the strain hardening exponent n to the frictional sliding response clearly appears as a dominant factor for such ductile materials. The relative influence of each parameter will be further quantified using results from the complete parametric study.

Before presenting these parameterized results, two additional remarks are appropriate here. Instead of using h_p/h_r to characterize the pile-up behavior, alternative formulations could have been based on pile-up volume. However, calculations showed that this volume varies only slightly with respect to material properties. Such limited dependence can be easily understood from the law of volume conservation that would apply in steady state if there were no residual volume variations due to the presence of residual stresses. Finally, details need to be given regarding the calculation of h_p and a_r from the position of individual nodes in the finite element discretization. The measure of h_p is taken as the height at which the width of the pile-up peak reached the horizontal distance between adjacent nodes. Such procedure is believed to be the best possible way to eliminate fluctuations associated with different sharpness and symmetry characteristics of the node profiles. (For any set of simulation results, the peak of the profile can be sharp with a single node at the tip, blunted with two nodes at nearly the same maximum height, or anywhere in-between those two opposite cases.) For the same reason, a_r was corrected for symmetry by measurements made from the mid-position of the horizontal segment drawn to determine h_p. These corrections did not change individual measurements by more than 5%, but they significantly reduced random fluctuations in H_s and h_p/h_r.

3.2. Dependence of the dimensionless functions on material parameters

The effect of plastic strain hardening exponent on the frictional sliding response was studied for seven different values of n: 0, 0.02, 0.06, 0.1, 0.2, 0.35 and 0.5. For each n value, the initial normalized yield strength
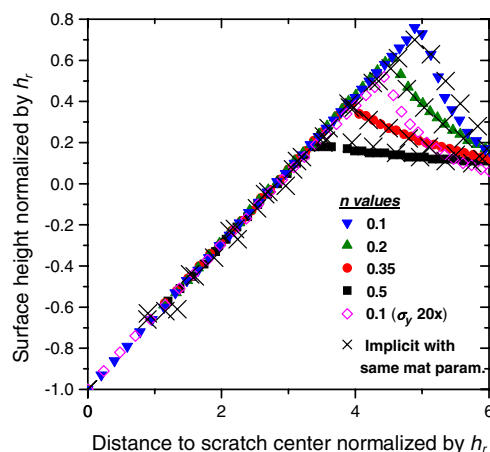

Fig. 4. Residual surface profile as a function of strain hardening exponent for $\sigma_y/E^* = 0.001$. The profile for a material with $n = 0.1$ and $\sigma_y/E^* = 0.02$ is also included to describe the effect of initial yield strength. Also shown with cross-hairs are the simulation results from the implicit method for $\sigma_y/E^* = 0.001$ and the different values of n.

σ_y/E was varied by at least an order of magnitude. Following the general trend observed in most material systems, the softest materials were studied up to the highest hardening rates whereas very hard materials were studied predominantly in the regime of low hardening rates. A set of 70 material property combinations was constructed to cover homogeneously the range of material property space indicated in Table 2. To obtain this range and to verify the scaling assumption for the use of the ratio σ_y/E, the properties were independently varied in the range of 20–7000 MPa for σ_y and from 4 to 600 GPa for E.

The dependence on these material parameters of the dimensionless functions defined in Section 2.2 (Eqs. (10)–(12)) was determined from the FEM results obtained with this set of properties. For the function Π_β describing the pile-up behavior and the function Π_γ describing the friction behavior, logistic functions were employed to describe the dependence on n and σ_y/E^*. Although there could be fundamental justifications for employing these functions, the practical advantage and improved accuracy obtained by using them was considered here as a major advantage. In addition, these functions use only a small number of fitting parameters and they allow to capture the asymptotic behavior.

For the determination of any of the three dimensionless functions, the numerical solutions were obtained by error minimization at two distinct steps. The first step was for the fitting with respect to σ_y/E^* that was done independently for each value of n, whereas the second step consisted in fitting with respect to n the different coefficients obtained in the first step. Small adjustments were introduced through a series of iterations aimed at enduring the most monotonic dependence on n for the sub-functions established in step 2 while maintaining fidelity to the FEM data.

In the following figures, these functions are plotted as continuous lines for five different values of strain hardening exponent. Also plotted are the individual data points obtained from finite element results and the analysis procedures described in Section 2.3. Fig. 5 is for the function Π_α, the normalized scratch hardness H_s/σ_y as a function of the normalized yield strength σ_y/E^*,

$$\Pi_\alpha\left(n, \frac{\sigma_y}{E^*}\right) = \left(\frac{H_s}{\sigma_y}\right) = \alpha1(n)\left(\frac{\sigma_y}{E^*}\right)^{\alpha2(n)} \tag{15}$$

with

$$\alpha1(n) = 3.32 - 5.79n + 2.8n^2,$$

and

$$\alpha2(n) = 0.07 - 1.283n + 0.248n^2.$$

This simple exponential function fits the data with high accuracy throughout the material space covered. A certain amount of scatter is observed for the FEM data set. With the relative error doubling when the hardness is calculated from the contact radius, even a small fluctuation in the contact radius, inherent to space discretization, can explain this scatter. Assuming the absence of bias on the fluctuations, they should not affect significantly the determination of the dimensionless function Π_α, the normalized hardness H_s/σ_y dimensionless function. For low hardening materials with n below 0.1, Π_α presents a relatively limited dependence on the normalized yield strength as the absolute value ranges from 2.5 to 4. Interestingly, this range of hardness to yield strength ratio is similar to the range from 2.6 to 3 typical found in normal indentation tests on hard

Table 2
Range of elasto-plastic properties covered by the parametric finite element study

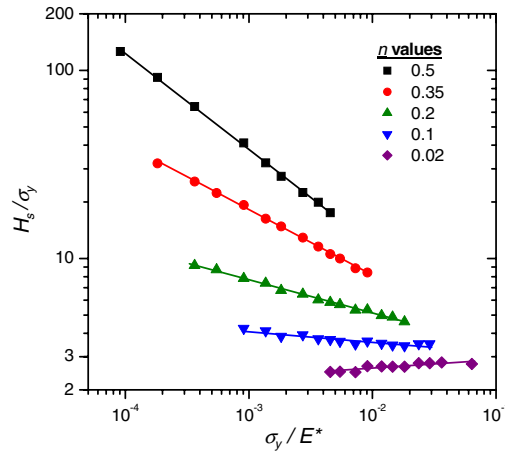| n	σ_y/E	
	Min	Max
0	0.01	0.1
0.02	0.005	0.07
0.06	0.002	0.04
0.1	0.001	0.032
0.2	0.0004	0.02
0.35	0.0002	0.01
0.5	0.0001	0.005

Fig. 5. Normalized scratch hardness as a function of normalized yield strength for five different values of the strain hardening exponent n. The curves represent the output from using the predicting Eq. (15).

materials. For larger values of the strain hardening exponent n, the ratio of H_s/σ_y increases significantly as does its dependence on σ_y/E^*. The predictions for the property dependence reported for indentation hardness follow a similar trend (Cheng and Cheng, 1998a,b). However, the magnitude of the dependence reported here for frictional sliding is several times larger. Such a difference can be explained by a difference in the magnitude of the plastic strain under the indenter. A more detailed discussion about the relationships between normal indentation and frictional sliding will be presented in Section 4.1 after the discussion of the effect of plastic flow properties on the pile-up and frictional response.

The second function, Π_β, is for the dependence of the normalized pile-up height on the elasto-plastic properties:

$$\Pi_\beta\left(n, \frac{\sigma_y}{E^*}\right) = \frac{h_p}{h_r} = \Pi_{\beta,\mathrm{RP}}(n) \left/ \left[1 + \left(\frac{\sigma_y}{X_\beta(n)E^*}\right)^{p_\beta(n)}\right]\right. \tag{16}$$

with

$$\Pi_{\beta,\mathrm{RP}}(n) = 0.904 - 1.684n + 1.987n^2 - 2.722n^3,$$
$$X_\beta(n) = 0.0378 - 0.2129n + 1.145n^2 - 3.34n^3 + 3.54n^4,$$

and

$$p_\beta(n) = -0.68\ln(n + 0.02).$$

This numerical function is plotted as five different continuous lines in Fig. 6, each line representing a specific value of the strain hardening exponent n. Such representation illustrates the fit with the original FEM data points and how the he pile-up height decreases with an increase in yield strength. For the range of σ_y/E^* covered, it also indicate a pronounced influence of the strain hardening exponent for all values of σ_y/E^*. An important effect of the strain hardening exponent was already depicted in Fig. 4, but only for a specific value of σ_y/E^*.

For low values of σ_y/E^*, the rigid-plastic asymptote was nearly achieved at most values of the strain hardening exponent n. For large values of σ_y/E^*, the curves and the data were truncated for $n \geqslant 0.35$. Such procedure limits the analysis to the cases where there is pile-up formation during scratching. The phenomenon of sink-in still leaves a residual pile-up, but the radius of residual contact does not correspond with the position of maximum height on the residual profile, requiring a more sophisticated analysis than the one presented here. This necessary truncation can explain why the elastic-limit of no residual pile-up was not approached except for the low hardening case. For $n = 0.02$, the curve clearly indicated a change from a negative to a positive inflection.
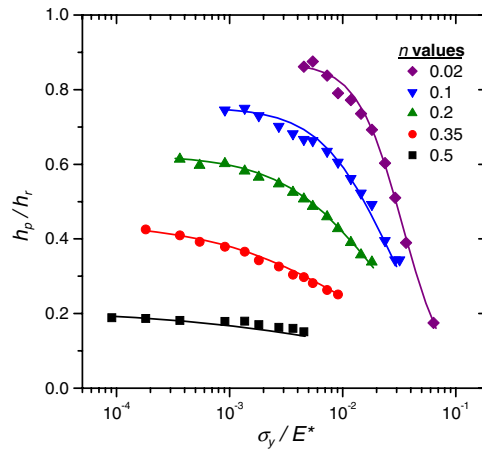
Fig. 6. Normalized pile-up height as a function of normalized yield strength for five different values of the strain hardening exponent n. The curves represent the output from using the predictions of Eq. (16).

To exemplify the relative contribution of n and σ_y/E^*, we consider a typical soft metallic alloy with $n = 0.1$ and $\sigma_y/E^* = 0.001$. A decrease in the characteristic h_p/h_r of that alloy from approximately 0.75 to 0.6 can occur either if n increases by twofold or if σ_y is increased by an order of magnitude, indicating a significantly more pronounced effect of increasing hardening exponent on h_p/h_r. However, although h_p/h_r is a complementary measurement that characterizes the frictional sliding response, the normalized pile-up height does not provide the pressure bearing capability of the material. In fact, the scratch hardness of the alternative material with $n = 0.2$ would be about four times smaller than the one for which σ_y would be increased by an order of magnitude.

In view of the lack of any prior experimental data or computational predictions for the effect of plastic hardening on H_s/σ_y and h_p/h_r, the results presented in this paper can only be compared with the predictions of Bucaille et al. (2001) and Bucaille and Felder (2002) for perfectly plastic materials. For the same indenter geometry, quantitative agreement is found for the hardness values. For the normalized pile-up height, the predictions are similar for materials with low hardening but the height predictions for large σ_y/E^* were significantly lower in the previous study (Bucaille et al., 2001; Bucaille and Felder, 2002). Since the friction coefficient for normal contact increases the pile-up height in frictional sliding because of the directionality of plastic flow, part of this difference could be accounted for by the assumption of frictionless contact in references (Bucaille et al., 2001; Bucaille and Felder, 2002). However, the former study used an implicit scheme with a constant depth. Therefore, it is possible that a change in the trajectory used to reach steady state, as described here in Section 2.3, would also lead to increased h_p/h_r to corroborate with the results presented here.

As a third parameter to characterize the frictional sliding response, the overall friction coefficient and the materials property dependence of its respective dimensionless function Π_γ were also determined. Fig. 7 presents the FEM data and this function

$$\Pi_\gamma\left(n, \frac{\sigma_y}{E^*}\right) = \left(\frac{F_t}{P}\right) = \mu_s = \Pi_{\gamma,\mathrm{RP}} \left/ \left[1 + \left(\frac{\sigma_y}{X_\gamma(n)E^*}\right)^{p_\gamma(n)} \right] \right. \tag{17}$$

with

$$\Pi_{\gamma,\mathrm{RP}} = 0.416,$$
$$X_\gamma(n) = 0.1149 - 0.2378n + 0.0954n^2,$$
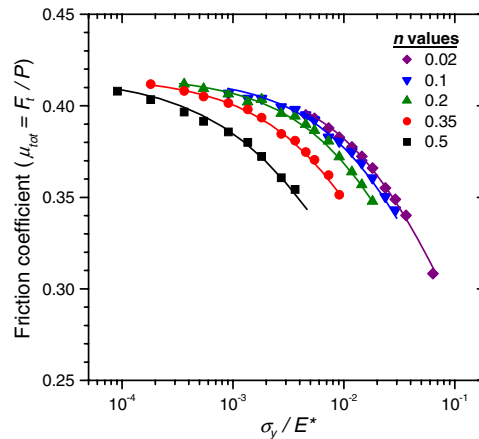
and

$$p_\gamma(n) = 0.8 - n^2/2.$$

Fig. 7. Effect of normalized yield strength and strain hardening exponent on the overall friction coefficients. The curves represent the output from using the predicting Eq. (17).

This overall ratio of tangential to normal force contains information about the friction for the local normal contact between surfaces and also about the contact geometry. The contribution from friction in normal contact should be equal to the coefficient μ_a, which is 0.15 for all the cases presented here. The contribution for the tangential pressure applied towards upstream would depend on the actual contact geometry and the plastic flow field.

With respect to material properties, μ_{tot} varies just the same way as h_p/h_r except that the magnitude of the variation is significantly less. Such a smaller dependence can be explained by a concurrent increase in tangential and normal pressure as the area of contact increases due to a higher pile-up. Within a limited range of yield strength and for n below 0.2, the predictions presented here suggest that any intrinsic effect of material plastic flow properties would fall within the scatter associated with surface preparation, material homogeneity and friction. This prediction might appear inconsistent with several previous studies that showed changes in friction coefficient between distinct but similar materials (Guzman et al., 1996; Bolduc et al., 2003; Hanlon et al., 2005a,b). However, these studies are generally carried out with a spherical tip in which case the geometry and the contact angle changes with penetration depth and pile-up height, therefore making the isolation of material properties more difficult.

An additional remark is in order here regarding the process of pile-up formation. It is well known from previous literature on machining (Gane and Skinner, 1973; Tsukizoe and Sakamoto, 1975; Black et al., 1988, 1990) that there is a critical apex angle θ below which the plastic deformation process transitions from ductile ploughing to chipping or machining. Although quantitative information is unavailable, it is very likely that this transition would occur at a larger angle θ for materials that have a strong tendency to form large and steep pile-up. Using the finite element models developed in this study, attempts were made to cover softer materials that would be nearly perfectly plastic while maintaining μ_a and θ to their fixed values. However, with n below 0.02 and σ_y/E^* below approximately 0.005, the normalized pile-up height h_p/h_r exceeded 0.9 and convergence required the imposition of special mesh gradients and control. It is believed that such material conditions were near this transition point for the geometry and friction conditions studied. If one were to characterize computationally or experimentally the behavior of softer perfectly plastic materials to ductile ploughing, μ_a and/or θ would probably need to be changed.

3.3. Experimental comparison

To compare the frictional sliding response of pure mc, ufc and nc nickel with the predictions from the parametric study, experiments were carried out under the same geometrical conditions. Using only pure nickel as a model, the effects of different phases and different friction coefficients were ruled out. In addition, carrying out the experiment at large loads eliminated the risk for surface and size effects. Because of the difference in

hardness of the different nickel samples and the fact that a constant load of 2 N was imposed in each case, the absolute dimensions of the width of the residual scratch $2a_r$ ranged from 60 μm for the mc nickel to 34 μm for the nc nickel. Additional tests carried out at different loads indicated that the response was not significantly dependent on the size of the indenter impression.

After the experiment, the pile-up height h_p and the residual depth h_r were determined from the maximum height and maximum depth obtained after linearly interpolating for the position of the original surface obtained from profilometry. The points used for this interpolation were away from the scratch center at a distance of four times the residual radius of contact ($4a_r$). With a very limited curvature and a slope below 2° for the original surface, this correction procedure was considered the most simple and reproducible alternative.

Using this procedure, individual values of a_r, h_p and h_r were obtained for each of cross-sectional profiles obtained from scanning at least five independent scratches. Typically, the difference in the average value obtained from independent experiments did not exceed 5%. However, for a given set of data associated with a single experiment, the standard deviation could reach up to 20% for the normalized pile-up height h_p/h_r. Such level of fluctuation corroborates well the oscillations in the process of pile-up formation and clearly emphasizes the need for a sample size of at least 25 data points.

For all three dimensionless parameters associated with the functions Π_α, Π_β and Π_γ, Table 3 presents a detailed comparison between the finite element predictions and the average values from the experimental results. With a difference of at most 7% between the predictions and the results, the finite element predictions appear to capture very well the trends as well as the absolute values of the scratch parameters H_s, h_p/h_r and μ_{tot}. Fig. 8 compares individual experimental scratch profiles obtained for the mc and nc pure nickel samples. Five individual profiles (open symbols) are presented for each test condition. In agreement with the predictions shown for these materials based on their plastic flow properties (cf. Table 3), the pile-up for the

Table 3
Comparison between experimental results and predictions based on elasto-plastic properties

	Properties		H_s/σ_y			h_p/h_r			μ_{tot}		
	σ_y (MPa)	n	Exp.	FEM	Δ (%)	Exp.	FEM	Δ (%)	Exp.	FEM	Δ (%)
nc	1600	0.02	2.76	2.58	7	0.82	0.84	2	0.37	0.39	5
ufc	850	0.06	2.92	3.09	6	0.74	0.76	2	0.38	0.40	5
mc	170	0.19	7.92	8.11	2	0.64	0.63	2	0.38	0.41	7

The elasto-plastic properties were obtained from tensile tests reported elsewhere (Schwaiger et al., 2003; Hanlon, 2004; Hanlon et al., 2005a,b).
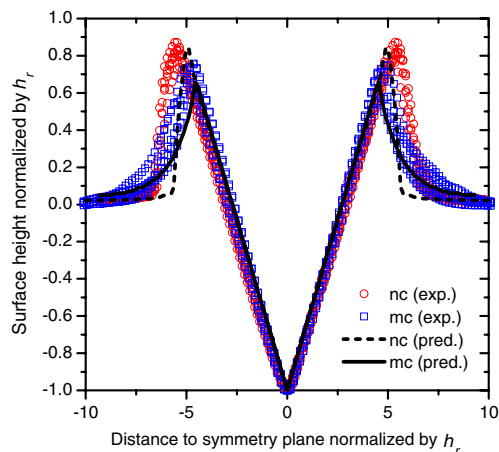

Fig. 8. Experimental profiles for pure nc and mc nickel. The lines represent predictions for these materials based on the plastic flow properties listed in Table 3.

nanocrystalline nickel has a higher ratio of h_p/h_r and presents a higher slope in the region of $r > a_r$. However, although the predictions for the height of the pile-up match with the experimental results, the experimental profiles appear more blunted. Such blunting could be due to surface natural oxide, surface tension and indentation size effects that were not taken into account by the finite element models.

4. Discussion

In this study, we developed a new framework to analyze the material behavior in frictional sliding. For the contact between a hard conical indenter and a fixed apex angle, it is proposed to use the scratch hardness and the normalized pile-up height to relate the response with elasto-plastic properties.

4.1. Predicting the scratch behavior using the universal functions

A special attention was given to ensure numerical accuracy. From a computational standpoint, the explicit/Eulerian scheme used in the analysis was well tested for its elastic limit and by comparing the results with those obtained with explicit/Lagrangian and implicit/Lagrangian schemes. From an experimental standpoint, all the measurements were carried out after a direct calibration of the instrument through the use of standard weights for the force measurements and of standardized surface patterns for the residual profile data. Under these conditions, the set of dimensionless functions presented in this study is expected to be relatively accurate and to correspond well with what would be the theoretical solution for this complex contact mechanics problem.

The comparison between the FEM results and the experimental results on the pure nickel model material system showed a strong agreement, both in terms of trends and absolute values. In fact, the relative difference was well below the computational variability associated with space discretization and the experimental variability inherent to the processes associated with microscale elasto-plastic contacts. And in other independent studies, a good correspondence was also observed between the predictions and the experimental results with pure copper over a wide range of different grain sizes and with aluminum alloys having different dispersion hardening precipitates.

Now assuming a good accuracy for the results from FEM, the accuracy of the dimensionless functions would depend on the ability of the fitting functions to correctly interpolate between the data points. For the interpolation with respect to σ_y/E^*, a careful inspection of Figs. 5–7 should provide a convincing argument. For the interpolation with respect to n, it should be noted that all the sub-functions are very smooth with a limited curvature. Through the use of these sub-functions, accuracy should be obtained in the range covered by the FEM data. This range of properties can be approximated by

$$(4.8 \times 10^{-5}) n^{-1.22} < \left(\frac{\sigma_y}{E^*} \right) < (5.5 \times 10^{-2}) e^{-5.11n}, \quad \text{where } 0 \leqslant n \leqslant 0.5 \tag{18}$$

or determined by inspection of Table 2. This range encompasses a great variety of the elasto-plastic properties found in practice. However, the numerical functions may not be accurate outside the specified range or when the plastic flow behavior greatly differs from power law strain hardening.

Π_α and Π_β were both found to simultaneously depend on σ_y/E^* and n. Using Eqs. (15) and (16), a complete sensitivity analysis was carried out for this effect of material properties. Table 4 presents the maximum percent

Table 4
Sensitivity analysis for the effect of variations in material properties on the predictions from the dimensionless functions

	Effect of σ_y				Effect of n			
	On H_s/σ_y		On h_p/h_r		On H_s/σ_y		On h_p/h_r	
	+5%	−5%	+5%	−5%	+5%	−5%	+5%	−5%
$n \leqslant 0.1$	5.3	−5.3	−4.7	4.8	3.4	−3.3	−1.8	1.9
$n = 0.2$	4.1	−4.1	−2.4	2.5	7.6	−7.1	−3.3	3.4
$n = 0.35$	3.2	−3.3	−1.4	1.5	13.3	−11.9	−7.0	7.4
$n = 0.5$	2.4	−2.5	−0.7	0.8	18.8	−16.2	−21.0	20.1

variation that can result from independently varying σ_y/E^* or n by $+/-5\%$. In most cases, these variations are less than twice those applied to the input parameters and they were found to be rather independent of the absolute value of σ_y/E^*, but their dependence on the absolute value of the strain hardening exponent was significant. For $n \leqslant 0.2$, the maximum variation in the predictions is similar or smaller than the variation in the material properties specified, but for higher n values the dependence intensifies for the effect of variations in n whereas it decreases for the effect of variations in σ_y/E^*. As n increases, its contribution to the magnitude of the flow stress also increases and so does the sensitivity of the predictions for H_s/σ_y and h_p/h_r. However, this increased sensitively still falls within the range of four times the error on the input parameters. For all the material property cases covered in this study, frictional sliding response can be predicted with an accuracy of the same order of magnitude as the accuracy on the input data for the material properties.

4.2. Representative plastic strain and comparison with normal indentation

The concept of representative strain has been used in recent studies on indentation (Giannakopoulos and Suresh, 1999; Dao et al., 2001; Chollacoop et al., 2003; Cao and Lu, 2004a,b; Ogasawara et al., 2005; Wang et al., 2005) for the amount of a characteristic plastic strain and the associated flow stress. The value is defined as the strain at which you can best establish a direct relationship between the hardness and the representative flow stress. Through this process, the variables σ_y/E^* and n are grouped into a single one that relates to the representative stress. As previously stated (Dao et al., 2001), the discrepancy in the values reported in the different studies can be explained by the differences in the definition used. For instance, the values determined using the loading curvature of the (P–h) response are significantly lower than the 8–10% found both numerically (Dao et al., 2001) and experimentally (Tabor, 1951) for the traditional definition of hardness based on the residual area of contact.

The concept of representative strain is used in normal indentation for extracting material properties, but here the main purpose of using it is to compare the magnitude of the strain field between indentation and frictional sliding. We used the traditional definition of the scratch hardness and tried to merge the variables. It appeared impossible to achieve a maximum error of less than 5% while trying to cover the full range of n values with a single value of ε_{rep}. Therefore, the material properties space covered was split into two. For the first domain, which includes all the data for $n \leqslant 0.2$ along with data for $\sigma_{rep}/E^* < 0.018$ and $n = 0.35$, the evolution of the scratch hardness with respect σ_{rep}/E^* becomes approximately n independent when normalized by the flow stress at 33.6% plastic strain. This fitting is shown in Fig. 9 along with a second plot made with a lower ε_{rep} of 15.5%. To ensure that all the possible combinations of material properties are covered within the range $0.2 < n < 0.35$, for this second domain data for $n = 0.2$ and $\sigma_{rep}/E^* > 0.016$ were added to the set of data for
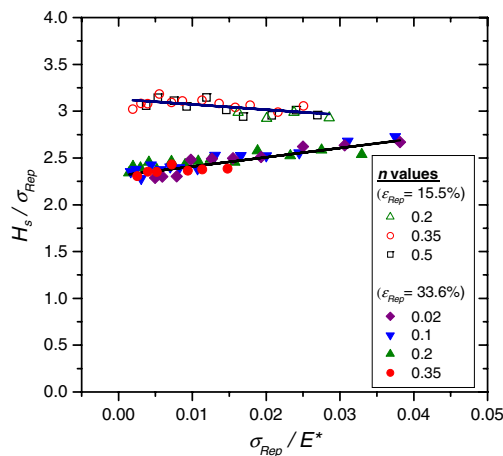

Fig. 9. Scratch hardness normalized by the flow stress at two distinct representative strains. The lower curve is for the first material property domain for which $\varepsilon_{rep} = 33.6\%$ fits best the data, whereas the upper curve is for the second property domain and $\varepsilon_{rep} = 15.5\%$.

$\geqslant 0.35$. By separating the material space, the maximum error felt below 4.2% and 3.2% for the plots with ε_{rep} of 33.6% and 15.5%, respectively.

Especially when a significantly different value of ε_{rep} is needed to cover the full material property space, this representative strain determined by error minimization may well be more of a mathematical convenience than a characteristic physical quantify. Ogasawara et al. (Ogasawara et al., 2005) have shown that ε_{rep} would be more appropriately defined by approximating the strain field in normal indentation is biaxial. This alternative procedure was also employed in the current study, but Table 5 shows no reduction in the fitting error. Also, the biaxial strain assumption did not allow carrying out a fit with a single ε_{rep} for all the sets of material properties. One possible explanation for this result is the predominant shear mode of deformation that prevails during frictional sliding with the geometry studied here and a low hardening exponent n. But independently of whether ε_{rep} is associated with a true characteristic plastic strain or eigenvalue, its usage does provide simplified expressions for the scratch hardness

$$\left(\frac{H_{\text{s}}}{\sigma_{33.6\%}}\right) = 9.88\left(\frac{\sigma_{33.6\%}}{E^*}\right) + 2.31 \Longleftrightarrow n \leqslant 0.2 \quad \text{or} \quad n \leqslant 0.35 \text{ and } \left(\frac{\sigma_{33.6\%}}{E^*}\right) < 0.018 \tag{19}$$

or

$$\left(\frac{H_{\text{s}}}{\sigma_{15.5\%}}\right) = -5.64\left(\frac{\sigma_{15.5\%}}{E^*}\right) + 3.13 \Longleftrightarrow n \geqslant 0.35 \quad \text{or} \quad n \geqslant 0.2 \text{ and } \left(\frac{\sigma_{15.5\%}}{E^*}\right) > 0.016, \tag{20}$$

and also provides a basis for comparison with normal indentation under the same geometrical conditions. Such a comparison is included in Table 5 with literature data based on the loading curvature of the P–h response as well as based on the traditional definition of hardness. Based on the foregoing analysis and for a strain hardening exponent n below 0.2, the representative strain associated with frictional sliding would be approximately four times as high as the one induced by normal indentation.

4.3. Practical use and limitations of instrumented single scratch tests

A fourfold increase in the amount of plastic strain obtained by using frictional sliding offers a greater capability to study effects of microstructure on the plastic flow process than with indentation. These effects could include strain-induced grain growth, partial crystallization or localized damage induced by the high residual tensile stress components. The residual tensile stresses are particularly high on the surface of the residual scar, especially near the point of contact with the indenter. The continuum mechanics approach employed is directly applicable to a large array of practical testing conditions where the material characteristic deformation length scale is finer than the experimental length scale. The approach could also be adapted to involve size-scale effects, but the solution would become more material specific.

From a perspective of measuring plastic properties at a sufficiently large length scale, the frictional sliding technique amplifies the effect of the strain hardening exponent on the normalized pile-up height. Whereas the maximum ratio of $h_{\text{p}}/h_{\text{r}}$ is of the order of 0.3 for normal indentation (Cheng and Cheng, 1998a,b), this ratio can vary from 0.2 to 0.9 for the range of material properties covered in the current study. Also, the surface

Table 5
Summary of the different values obtained for ε_{rep} by using the uniaxial and/or bixial strain assumption (also shown are literature data for instrumented indentation)

		Based on ε_{p} (uniaxial/shear)		Based on $2\varepsilon_{\text{p}}$ (biaxial)	
		ε_{rep} (%)	Max error (%)	ε_{rep} (%)	Max error (%)
Current study	Property domain #1	33.6	4.2	16.9	4.3
	Property domain #2	15.5	3.2	7.7	3.2
Literature on indentation (Dao et al., 2001; Ogasawara et al., 2005)	Functional for loading curvature	3.3	2.9	1.15	NA
	Functional for residual area of contact	8.2	6.0	–	–

curvature in frictional sliding is always positive, leading to the formation of a pile of material in front of the indenter. It is much easier to measure an impression accurately with pile-up than with sink-in. Based on these considerations, it could be more suitable to use frictional sliding in conditions where the information from the residual profile would be used to establish relationships with properties.

Repeated measurements of h_p/h_r in frictional sliding can be more easily obtained by taking adjacent 2D profiles from the unloaded scratch instead of studying a full 3D pyramidal imprint. Procedures could be developed to measure the a_r and h_p by scanning the surface with the indenter tip itself, but such technique may not provide an accurate direct measurement of h_r. Preliminary experimental trials suggested that the indenter can hardly reenter fully the residual scar without the application of a relatively high load. Therefore, measuring directly the residual profile appears as the most reliable approach to establish a relationship with mechanical properties.

A reverse analysis method to extract properties is currently being developed based on the dimensionless functions developed in this study. The establishment of such method requires to ascertain the effect of the friction coefficient in normal contact μ_a. Although the most commonly adopted value was used in the present study, the effect of this parameter on the frictional sliding response was also evaluated. Early calculations indicated a limited dependence for the normalized hardness H_s/σ_y, but a significant dependence for h_p/h_r. A comprehensive study is also underway to fully quantify the effect of μ_a in steady-state frictional sliding and will be presented elsewhere.

5. Conclusions

From this study of the frictional sliding response of elasto-plastic materials, the following conclusions are drawn.

1. The frictional sliding response of elasto-plastic materials in contact with a hard conical tip can be predicted with an accuracy of the same order as the accuracy of the input data for the material properties. The material properties needed are the Young's modulus, the Poisson's ratio, the initial yield strength and the plastic strain hardening exponent.
2. As for the indentation hardness, the hardness in frictional sliding of elastic–perfectly plastic materials is between 2.5 and three times the yield strength. However, non-linear effects become progressively more significant as the plastic strain hardening exponent increases and the magnitude of the change in hardness becomes several times larger than the one reported for normal indentation. Also, the pile-up height in frictional sliding can be as much as three times as high as the one obtained through normal indentation and a transition from pile-up to sink-in occurs only at much greater values of the hardening exponent.
3. The overall friction coefficient decreases slightly with an increase in yield strength or strain hardening exponent, but for most cases the magnitude of the change would fall within the experimental scatter. This finding is specific to the contact with a conical tip where the assumption of size-independent material properties allows for the use of geometrical scaling. It does not apply to the contact with a spherical tip where the geometrical contribution of the penetration depth on the friction coefficient can lead to a misinterpretation of experimental results.
4. In frictional sliding, the pile-up height and the hardness are the response parameters that are the most sensitive to the plastic flow properties. Further research is underway to develop an engineering method for estimating experimentally these properties.

A simple scratch test induces a localized plastic flow process that can be modeled, reproduced experimentally and used for material characterization. It can also provide quantitative insights into understanding the contact conditions that are closer to those generated in actual tribological events than possible with instrumented normal indentation.

Acknowledgement

References

Alcala, J., Barone, A.C., Anglada, M., 2000. Influence of plastic hardening on surface deformation modes around vickers and spherical indents. Acta Materialia 48 (13), 3451–3464.

Atkins, A.G., Tabor, D., 1965. Plastic indentation in metals with cones. Journal of Mechanics and Physics of Solids 13 (3), 149–164.

Black, A.J., Kopalinsky, E.M., Oxley, P.L.B., 1988. Investigation of the different regimes of deformation which can occur when a hard wedge slides over a soft surface: the influence of wedge angle, lubrication and prior plastic working of the surface. Wear 123 (1), 97–114.

Black, A.J., Kopalinsky, E.M., Oxley, P.L.B., 1990. Sliding metallic friction with boundary lubrication. An investigation of a simplified friction theory and of the nature of boundary lubrication. Wear 137 (2), 161–174.

Bolduc, M., Terreault, B., Reguer, A., Shaffer, E., St-Jacques, R.G., 2003. Optimum tribological improvement of aluminum using oxygen plasma source ion implantation. Journal of Materials Research 18 (8), 1761–1764.

Bowden, F.P., Tabor, D., 1950. The friction and lubrification of solids. Oxford University Press, Oxford.

Briscoe, B.J., Biswas, S.K., Sinha, S.K., Panesar, S.S., 1993. Scratch hardness and friction of a soft rigid-plastic solid. Tribology International 26 (3), 183–193.

Bucaille, J.L., Felder, E., 2002. Finite-element analysis of deformation during indentation and scratch tests on elastic–perfectly plastic materials. Philosophical Magazine A – Physics of Condensed Matter Structure Defects and Mechanical Properties 82 (10), 2003–2012.

Bucaille, J.L., Felder, E., Hochstetter, G., 2001. Mechanical analysis of the scratch test on elastic perfectly plastic materials with the three-dimensional finite element modeling. Wear 249 (5–6), 422–432.

Bucaille, J.L., Stauss, S., Felder, E., Michler, J., 2003. Determination of plastic properties of metals by instrumented indentation using different sharp indenters. Acta Materialia 51 (6), 1663–1678.

Cao, Y.P., Lu, J., 2004a. Depth-sensing instrumented indentation with dual sharp indenters: stability analysis and corresponding regularization schemes. Acta Materialia 52 (5), 1143–1153.

Cao, Y.P., Lu, J., 2004b. A new method to extract the plastic properties of metal materials from an instrumented spherical indentation loading curve. Acta Materialia 52 (13), 4023–4032.

Cheng, Y.-T., Cheng, C.-M., 1998a. Effects of 'sinking in' and 'piling up' on estimating the contact area under load in indentation. Philosophical Magazine Letters 78 (2), 115–120.

Cheng, Y.-T., Cheng, C.-M., 1998b. Scaling approach to conical indentation in elastic–plastic solids with work hardening. Journal of Applied Physics 84 (3), 1284.

Cheng, Y.-T., Li, Z., Cheng, C.-M., 2002. Scaling relationships for indentation measurements. Philosophical Magazine A: Physics of Condensed Matter, Structure, Defects and Mechanical Properties 82 (10), 1821–1829.

Cheng, Y.T., Cheng, C.M., 2004. Scaling, dimensional analysis, and indentation measurements. Materials Science & Engineering R-Reports 44 (4–5), 91–149.

Chollacoop, N., Dao, M., Suresh, S., 2003. Depth-sensing instrumented indentation with dual sharp indenters. Acta Materialia 51 (13), 3713–3729.

Dao, M., Chollacoop, N., Van Vliet, K.J., Venkatesh, T.A., Suresh, S., 2001. Computational modeling of the forward and reverse problems in instrumented sharp indentation. Acta Materialia 49 (19), 3899–3918.

Dasari, A., Rohrmann, J., Misra, R.D.K., 2004. On the scratch deformation of micrometric wollastonite reinforced polypropylene composites. Materials Science and Engineering A 364 (1–2), 357–369.

Deuis, R.L., Subramanian, C., Yellup, J.M., 1996. Abrasive wear of aluminium composites – a review. Wear 201 (1–2), 132–144.

Fang, L., Cen, Q., Sun, K., Liu, W., Zhang, X., Huang, Z., 2005. FEM computation of groove ridge and Monte Carlo simulation in two-body abrasive wear. Wear 258 (1–4), 265–274 (Special issue).

Fischer-Cripps, A.C., 2000. Introduction to Contact Mechanics. Springer-Verlag, New York.

Gane, N., Skinner, J., 1973. Friction and scratch deformation of metals on a micro scale. Wear 24 (2), 207–217.

Giannakopoulos, A.E., Suresh, S., 1999. Determination of elastoplastic properties by instrumented sharp indentation. Scripta Materialia 40 (10), 1191–1198.

Guzman, L., Bonini, G., Adami, M., Ossi, P.M., Miotello, A., Vittori-Antisari, M., Serventi, A.M., Voltolini, E., 1996. Mechanical behaviour of nitrogen-implanted aluminum alloys. Surface & Coatings Technology.

Hanlon, T., 2004. Grain Size Effects on the Fatigue Response of Nanocrystalline Materials. Ph.D. Thesis. Department of Materials Science and Engineering. Cambridge, MIT.

Hanlon, T., Chokshi, A.H., Manoharan, M., Suresh, S., 2005a. Effects of grain refinement and strength on friction and damage evolution under repeated sliding contact in nanostructured metals. International Journal of Fatigue 27 (10–12), 1159–1163.

Hanlon, T., Tabachnikova, E.D., Suresh, S., 2005b. Fatigue behavior of nanocrystalline metals and alloys. International Journal of Fatigue 27 (10–12), 1147–1158.

Hutchings, I.M., 1992. Tribology: Friction and Wear of Engineering Materials. CRC Press, Kent.

Johnson, K.L., 1985. Contact Mechanics. Cambridge University Press, London.

Kumar, K.S., Van Swygenhoven, H., Suresh, S., 2003. Mechanical behavior of nanocrystalline metals and alloys. Acta Materialia 51 (19), 5743–5774.

Liang, Y.N., Ma, Z.Y., Li, S.Z., Li, S., Bi, J., 1995. Effect of particle size on wear behaviour of sic particulate-reinforced aluminum alloy composites. Journal of Materials Science Letters 14 (2), 114–116.

Maeda, K., Bismarck, A., Briscoe, B.J., 2005. Mechanisms of scratching frictions and damage maps for rubber compounds. Wear 259 (1–6), 651–660.

Marx, V., Balke, H., 1997. Critical investigation of the unloading behavior of sharp indentation. Acta Materialia 45 (9), 3791–3800.

Mata, M., Alcala, J., 2003. Mechanical property evaluation through sharp indentations in elastoplastic and fully plastic contact regimes. Journal of Materials Research 18 (7), 1705–1709.

Matsuda, K., 2002. Prediction of stress–strain curves of elastic–plastic materials based on the vickers indentation. Philosophical Magazine A: Physics of Condensed Matter, Structure, Defects and Mechanical Properties 82 (10), 1941–1951 (Special issue).

Mesarovic, S.D., Fleck, N.A., 1999. Spherical indentation of elastic–plastic solids. Proceedings of the Royal Society of London Series A – Mathematical Physical and Engineering Sciences 455 (1987), 2707–2728.

Milman, Y.V., Galanov, B.A., Chugunova, S.I., 1993. Plasticity characteristic obtained through hardness measurement. Acta Metallurgica et Materialia 41 (9), 2532.

Misra, R.D.K., Hadal, R., Duncan, S.J., 2004. Surface damage behavior during scratch deformation of mineral reinforced polymer composites. Acta Materialia 52 (14), 4363–4376.

Mohamed Sani, R.B., Sinha, S.K., Ying Tan, J.P., Zeng, K.Y., 2005. Wear debris generation mechanism for polymers studied by nanoscratching. Philosophical Magazine 85 (19), 2101–2122.

Mohs, F., 1824. Gruudriss der Mineralogie (Treatise on Mineralogy, Eng. trans. by W. Haidinger, Transactions of the Royal Society of Edinburgh, published at Edinburgh in three volumes, 1825).

Ogasawara, N., Chiba, N., Chen, X., 2005. On the representative strain of indentation analysis. Journal of Materials Research 20 (8), 2225–2234.

Oliver, W.C., Pharr, G.M., 1992. An improved technique for determining hardness and elastic-modulus using load and displacement sensing indentation experiments. Journal of Materials Research 7 (6), 1564–1583.

Oliver, W.C., Pharr, G.M., 2004. Measurement of hardness and elastic modulus by instrumented indentation: advances in understanding and refinements to methodology. Journal of Materials Research 19 (1), 3–20.

Pharr, G.M., Oliver, W.C., Brotzen, F.R., 1992. On the generality of the relationship among contact stiffness, contact area, and elastic-modulus during indentation. Journal of Materials Research 7 (3), 613–617.

Revankar, G., 1990. Introduction to hardness testingAsm Handbook: Mechanical Testing and Evaluation, vol. 8. ASM International, Materials Park.

Sakai, M., Akatsu, T., Numata, S., Matsuda, K., 2003. Linear strain hardening in elastoplastic indentation contact. Journal of Materials Research 18 (9), 2087–2096.

Schwaiger, R., Moser, B., Dao, M., Chollacoop, N., Suresh, S., 2003. Some critical experiments on the strain-rate sensitivity of nanocrystalline nickel. Acta Materialia 51 (17), 5159–5172.

Storakers, B., Elaguine, D., 2005. Hertz contact at finite friction and arbitrary profiles. Journal of the Mechanics and Physics of Solids 53 (6), 1422–1447.

Subhash, G., Zhang, W., 2002. Investigation of the overall friction coefficient in single-pass scratch test. Wear 252 (1–2), 123–134.

Tabor, D., 1951. The Hardness of Metals. Clarendon press, Oxford.

Truman, C.E., Sackfield, A., Hills, D.A., 1995. Contact mechanics of wedge and cone indenters. International Journal of Mechanical Sciences 37 (3), 261–275.

Tsukizoe, T., Sakamoto, T., 1975. Friction in scratching without metal transfer. Bulletin of the JSME 18 (115), 65–72.

Tunvisut, K., Busso, E.P., O'Dowd, N.P., Brantner, H.P., 2002. Determination of the mechanical properties of metallic thin films and substrates from indentation tests. Philosophical Magazine A: Physics of Condensed Matter, Structure, Defects and Mechanical Properties 82 (10), 2013–2029 (Special issue).

Tunvisut, K., O'Dowd, N.P., Busso, E.P., 2001. Use of scaling functions to determine mechanical properties of thin coatings from microindentation tests. International Journal of Solids and Structures 38 (2), 335–351.

Wang, L., Ganor, M., Rokhlin, S.I., 2005. Inverse scaling functions in nanoindentation with sharp indenters: Determination of material properties. Journal of Materials Research 20 (4), 987–1001.

Wang, L., Rokhlin, S.I., 2005. Universal scaling functions for continuous stiffness nanoindentation with sharp indenters. International Journal of Solids and Structures 42 (13), 3807–3832.

Williams, J.A., 1996. Analytical models of scratch hardness. Tribology International 29 (8), 575–584.

Wilson, S., Hawthorne, H.M., Yang, Q., Troczynski, T., 2000. Sliding and abrasive wear of composite sol–gel alumina coated al alloys. Surface and Coatings Technology 133–134, 389–396.

Youn, S.W., Kang, C.G., 2004. A study of nanoscratch experiments of the silicon and borosilicate in air. Materials Science and Engineering A 384 (1–2), 275–283.

Youn, S.W., Kang, C.G., 2005. Erratum: "A study of nanoscratch experiments of the silicon and borosilicate in air (Materials Science and Enginering A (2004) vol. 384 (1–2) (275–283), doi:10.1016/j.Msea.2004.06.044). Materials Science and Engineering A 393 (1–2), 398.

Zhang, Z., Zhang, L., Mai, Y.-W., 1994. Modelling friction and wear of scratching ceramic particle-reinforced metal composites. Wear 176 (2), 231–237.

Zhang, Z.F., Zhang, L.C., Mai, Y.-W., 1995. Particle effects on friction and wear of aluminium matrix composites. Journal of Materials Science 30 (23), 5999–6004.